



Kinetics Performance for Cadmium (II) Ion Adsorption Using Mesoporous Silica Embedded with Iron Oxide

DESITA KAMILA ULFA¹ and MARIA ULFA¹

¹Chemistry Education Study Program, Faculty of Teacher Training and Education, Sebelas Maret University, Jl. Ir. Sutami 36A Surakarta, Central Java, Indonesia.

*Corresponding author E-mail: ulfa.maria2015@gmail.com

<http://dx.doi.org/10.13005/ojc/35Specialissue103>

Received: December 26, 2018; Accepted: February 02, 2019)

ABSTRACT

Mesoporous silica embedded with iron oxide successfully synthesized by wet impregnation following with microwave. Resulting material have characterized by XRD, FTIR, EDX, BET and TEM. The result showed that mesoporous silica morphology is the hexagonal structure-like with surface area is 470 m²/g, pore volume is 0.87 cc/g and pore diameter of 6.5 nm. The interesting phenomenon showed that the amount of iron particle on surface area is 25.47% which has high similarity with the weight of the adding iron during preparation. The most functional group that observed by FTIR in mesoporous silica sample are silanol Si-OH, Si-O-Si and Fe-O-Si. It was effectively used as an adsorbent for the adsorption of cadmium (II) ion. Mesoporous silica applied for cadmium ion which is carried out by cadmium solution with initial concentration was 23.97 mmol/L for 7 h at 25°C with stirring rate 150 rpm. The optimum contact time of the adsorption capacity was reached at 80 minutes. The optimum adsorption capacity for cadmium ions was 74.25 mmol/g fitted by kinetic models Lagergren. According to these results, mesoporous silica embedded with iron oxide could be a potential material for heavy metal removal process.

Keywords: Mesoporous Silica, Iron oxide, Cadmium (II) ion, Characterization, Adsorption, Kinetic models.

INTRODUCTION

One type of heavy metal that can pose a serious threat in the environment is cadmium, because it is toxic even in low concentrations of 0.0001 mg/L and cannot be decomposed¹. Cadmium can be produced by the disposal of waste from nickel-cadmium batteries, phosphate fertilizers, pesticides, pigments, dyes, oil refineries, plastics, welding and soldering, photography, iron, steel and cement

production². The overall production of cadmium in the world reaches 22.300 tons; the maximum concentration of cadmium for drinking water is 0.003 mg/L; and the cadmium working threshold that was previously set at 0.000100–0.000200 mg/L changed to 2 to 50 mg/L³. The World Health Organization (WHO) reveals disorders of the lungs, kidneys and carcinogens for humans can be caused by cadmium with levels more than normal⁴.



Some conventional methods can be used to remove cadmium metal ions including adsorption, chemical precipitation, ion exchange, membrane separation and solvent extraction⁵.

However, some of these methods have disadvantages such as the need for special or high energy reagents, removal of imperfect metals, and generation of waste products that contain other heavy metals which are sometimes more toxic⁶. One alternative choice for removing heavy metal cadmium ions is adsorption because it has high efficiency, no energy, is cheap and environmentally friendly⁷. Materials commonly used to remove heavy metal cadmium ions include husk-based carbon nuts, chitin, marine algae, bacteria, magnetic nanoparticles, zeolites and waste from boron enrichment plants (BW)⁷⁻¹⁴. The material is less effective to be used to adsorb cadmium metal ions because it has low adsorption ability, low surface area, low size and low porosity. Therefore an adsorbent is needed which has a higher surface area and porosity. Adsorbents that have high adsorption ability include mesopore zeolite, pillared clay, silica gel, and SBA-15¹⁵. Among inorganic materials on mesopore silica are materials that are widely used for adsorption¹⁶. Types of mesopore silica include M41S (MCM 41, MCM 50, MCM 48) and SBA-15¹⁷. Mesopore silica is the most effective material to be used to adsorb cadmium ions.

SBA - 15 is one of mesoporous material with unique character such as :a high surface area (~ 500 - 1500 m²/g), regular hexagonal structure, large pore diameter (~ 5-30 nm)^{18,24-28}. In addition, SBA-15 not only have inertness character but also high thermal stability, and easily in regeneration process. The difficulties of separation have been generated by small particle of mesoporous silica SBA-15 so its give impact for filtering the the adsorbate from adsorbent.²⁹⁻³¹ This problem can be overcome by adding substituents/metals that can help the separation process. Regeneration of SBA-15 as an adsorbent can be done by separating the adsorbate. This can be done by adding substituents/metals to the SBA-15 to assist the separation process. Some transition group metals such as Fe, Cr, and V can be used as separator substituents because they have high magnetic properties¹⁹. The separation process of mesoporous silica from the adsorbate have been rarely investigated.

In previous work, mesoporous silica embedded with iron oxide has been synthesized as adsorbent to remove cadmium (II) ion. In the best in our knowledge, cadmium (II) ion adsorption using mesoporous silica embedded with iron oxide have been rarely investigated by researchers. Mesoporous silica embedded with iron oxide is expected to produce a material that has a high adsorption capacity of cadmium (II) ion. Wet impregnation method was used to experiment because cheap, effective and efficient. The properties mesoporous silica embedded with iron oxide characterized by XRD, SEM, EDAX and FTIR. The adsorption performance of mesoporous silica embedded with iron oxide to cadmium (II) ion removal was investigate by Atomic Absorption Spectroscopy (AAS). The adsorption kinetic model such as Lagergren, Ho and McKay, Langmuir, and Freundlich models are used to evaluate adsorption capacity.

EXPERIMENTAL

Material

Tetra ethyl orthosilicate (TEOS) from merck millipore as silica source, poly(ethylene glycol)-block-poly(propylene glycol)-block-poly(ethylene glycol) EO₂₀-PO₇₀-EO₂₀ (P123) from millipore sigma as template agent and HCl 0.1 M solution were used to synthesize and activate SBA-15. Solution of HCl 37% was used to prepare HCl 0.1 M and 2 M solution. Cd(CH₃COO)₂·4H₂O (molar mass of 112 g/mol) and distilled water were used to prepare simulation solution cadmium (II). Fe(NO₃)₃·9H₂O from Sigma-Aldrich (hygroscopic with a molecular weight of 404 g/mol) is used to prepare solution Fe(NO₃)₃ 1 M.

Synthesis of SBA-15

Pluronic (P123) 3.6 g was dissolved in 150 g HCl 2 M at room temperature. The mixture was stirred for 4 h 150 rpm in closed conditions. Then, the mixture was dropped with 8.2 g TEOS (1 drop per 10 seconds) at room temperature while stirring. After that, the mixture was stirred for 20 h 150 rpm in closed condition. The mixture put in the hydrothermal reactor was heated at 100°C for 24 hours. The white solids were filtered and washed with distilled water to pH 7. They were dried in an oven at 100°C for 24 h and calcined at 550°C for 24 hours. The solids were stored in a plastic bottle.

Activation of SBA-15

Activation of mesoporous silica made by soaking the mesoporous silica in HCl 0.1 M for

24 hours. Solution of HCl 0.1 M was made by dissolving 8.2 mL of HCl 37% solution in distilled water. Then the results were filtered and dried at 100°C for 48 hours. Solution $\text{Fe}(\text{NO}_3)_3$ 1 M was prepared by $\text{Fe}(\text{NO}_3)_3 \cdot 9\text{H}_2\text{O}$ from Sigma-Aldrich as a precursor iron oxide. Mesoporous silica activated was mixed in solution $\text{Fe}(\text{NO}_3)_3$ 1 M as an adsorbent and stirred for 2 h 250 rpm at 25°C. The results were dried in oven for 24 h at 100°C and microwaved for 30 min at a high temperature, subsequently calcined at 750°C for 6 hours²⁰.

Characterization of mesoporous silica embedded with iron oxide

The adsorbent structure and physico-chemical composition were identified by some characterization. X-ray diffraction (Rigaku Multiflex 2 kW) identified the crystal structure in the Laboratory of Geological Engineering, Gadjah Mada University, Yogyakarta at 2 θ with a large angle between 10° to 80°. Spectrophotometer Fourier Transform Infra Red (Shimadzu Prestige-21) identified the functional groups of mesoporous silica embedded with iron oxide in Faculty of Math and Science Laboratory Sebelas Maret University. TEM identified the morphology of mesoporous silica and mesoporous silica embedded with iron oxide in Chemistry Laboratory, Faculty of Mathematics and Natural Sciences Gadjah Mada University. EDX (TSL AmateX) identified the elemental composition of mesoporous silica embedded with iron oxide were in the Characterization Division of the Faculty of Mathematics and Natural Sciences Institute of Sepuluh November.

Adsorption of Cadmium (II) ions

Simulation of solution cadmium 23.97 mmol/L were made by dissolving cadmium acetate which has the chemical formula $\text{Cd}(\text{CH}_3\text{COO})_2 \cdot 4\text{H}_2\text{O}$ and molar mass of 112 g/mol in distilled water as adsorbate. Solution HCl 0.1 M as an acid solution on the activation process of mesoporous silica.

The initial concentration of cadmium (II) solution was prepared by dissolving 2.772 g of $\text{Cd}(\text{CH}_3\text{COO})_2 \cdot 4\text{H}_2\text{O}$ with distilled water in a beaker until all solids are dissolved and then put in a 1000 mL volumetric flask and add distilled water to mark boundaries. Afterwards shaken until homogeneous. Mesoporous silica embedded with iron oxide as much as 0.005 g in 25 mL adsorbate included.

The solution was stirred at 150 rpm for 7 h at room temperature until it reaches equilibrium. Standard solution prepared by taking 10 pieces of 25 mL flask, each filled with 0.125; 0.1; 0.15; 0.20; 0.25; 0.30; 0.40; 0.45; and 0.50 mL of stock cadmium (II) solution. Then add distilled water to the mark and then shaken until homogeneous. The standard solution is measured using AAS to create a calibration curve. The adsorption capacity of cadmium (II), q_e (mmol/g), is calculated by the following equation

$$q_e = \frac{C_i - C_e}{w} \times V \quad (1)$$

With C_i and C_e are the concentration of cadmium (II) solution before and after adsorption (mmol/L), V is the volume of cadmium adsorbed solution (L), and w is the mass of mesoporous silica embedded with iron oxide (g). The experiments were performed at 25°C for 7 hours. The initial concentration of cadmium (II) solution was 23.97 mmol/L, samples were taken at regular intervals.

The adsorption capacity were analyzed by Lagergren, Ho and McKay, Langmuir, and Freundlich models. The Lagergren and Ho and McKay kinetic models are described by equation (2) and (3) respectively

$$\log(q_e - q_t) = \log q_e - kt \quad (2)$$

$$\frac{t}{q_t} = \frac{1}{k_2 \cdot q_e^2} + \frac{1}{q_e} \cdot t \quad (3)$$

With q_e is the equilibrium adsorption capacity (mg/g), q_t is the adsorption capacity at time t (mg/g), k is the Lagergren rate constant (min^{-1}), k^2 is the Ho and McKay rate constant (g/mg min) and t is contact time (min).

The adsorption capacity by Langmuir, and Freundlich models are expressed by equation (4) and (5) respectively

$$\log(q_e) = \log(K_f) + \log(C_e) \quad (4)$$

$$q_e = K_f C_e^{1/n} \quad (5)$$

With q_e is the equilibrium adsorption capacity (mg/g), C_e is the concentration in equilibrium (mmol/L), K_f and n are isotherm constants related to the adsorption capacity and adsorption intensity of adsorbent respectively.

RESULTS AND DISCUSSION

Figure 1 shows the X-ray diffraction pattern of mesoporous silica, iron oxide, and mesoporous silica embedded with iron oxide with a large angle 2θ . There are any peaks detected at 22° for iron oxide and mesoporous silica embedded with iron oxide. It is commonly detected in amorphous material. In addition, some peaks were detected on mesoporous silica embedded with iron oxide at 35.5° ; 43.4° ; 57.5° and 63° showed hematite (α - Fe_2O_3). This result is supported research by Martins, 2016²¹.

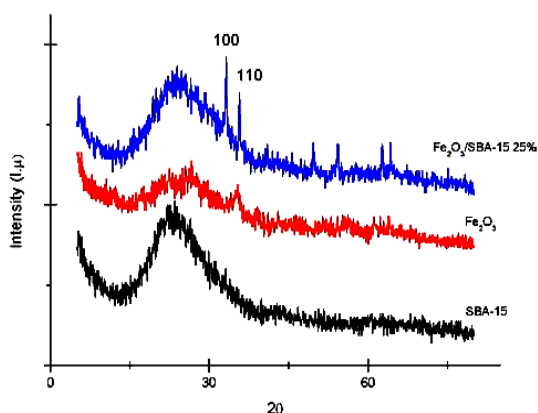


Fig. 1. Large angle XRD diffractogram mesoporous silica, iron oxide and mesoporous silica embedded with iron oxide

X-ray diffraction pattern with a small angle 2θ angle range between 1.0° to 0.8° on the scan speed $4^\circ/\text{min}$ shows three different reflection peak that is (1 0 0), (1 1 0), and (2 0 0) with the highest peak at an angle of 1.0° , 1.5° , and 1.8° material with hexagonal structure. The third peak showed a typical peak mesoporous structure similar to mesoporous silica. However, the reflection peak (2 0 0) at small angles 2θ are not visible. This can be due to a reduction in the surface area of mesoporous silica embedded with iron oxide process. It can also be due to a change in part Si by iron oxide. On the graph with large angle 2θ seen their peaks were detected at 22° for iron oxide and mesoporous silica embedded with iron oxide.

Figure 2 shows IR of mesoporous silica, iron oxide, and mesoporous silica embedded with iron oxide, the transmittance peak of mesoporous silica embedded with iron oxide is higher than mesoporous silica which indicates that the transmission energy of mesoporous silica embedded with iron oxide

larger than the transmission energy of mesoporous silica. In addition, the value of transmissi also shows adsorption energy mesoporous silica embedded with iron oxide smaller than mesoporous silica. It means that the addition of iron oxide will reduce the energy absorption of mesoporous silica (SBA-15)²².

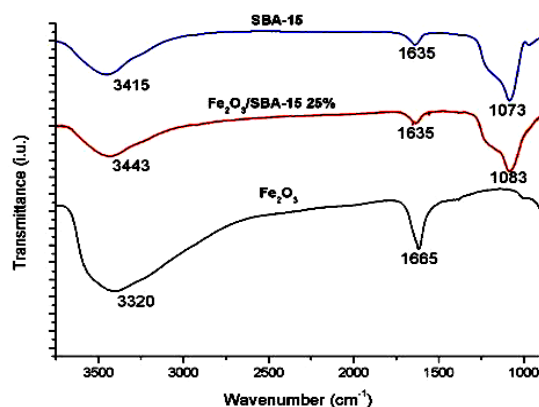


Fig. 2. IR spectra of mesoporous silica, iron oxide and mesoporous silica embedded with iron oxide

Table 1 in the IR spectrum indicate the presence of iron oxide vibration. It shows vibration force of Fe-O-Fe at 863 cm^{-1} with a width of 1.31 and a vibration force of Fe-O at 495 cm^{-1} with a width of 4.045. While vibration at 1028 cm^{-1} , 1138 cm^{-1} and 1235 cm^{-1} respectively indicates that iron particle reduced by oxygen of iron oxide. Peak width at 3443 cm^{-1} , 3446 cm^{-1} and 3416 cm^{-1} respectively representing vibrations OH of mesoporous silica embedded with iron oxide, mesoporous silica, and iron oxide. Mesoporous silica embedded with iron oxide, mesoporous silica, and iron oxide which can be caused by the presence of silanol or an OH group of molecules adsorbed water.

The graph in Fig. 3 shows the elements of mesoporous silica embedded with iron oxide, they are C, O, Si, Fe and Co elements. Mesoporous silica embedded with iron oxide adsorbent has the atomic volume (At) which amounted to 2.80%, 46.82%, 24.71%, 25.27%, and 0.40% for C, O, Si, Fe and Co elements. EDX spectrum of mesoporous silica embedded with iron oxideshows the iron particles is 25 wt%. Iron particle loaded on mesoporous silica shows that the impregnation process has been successfully carried out in which iron particle has embedding in mesoporous site. These results indicate that the compounds formed in the form of $\text{Fe}_2\text{O}_3/\text{SBA-15}$. It is based on a comparison of the atomic volumes percent with the relative atomic

mass of $\text{Fe}_2\text{O}_3/\text{Si}$ which indicates the amount of Fe is less than O and Si.

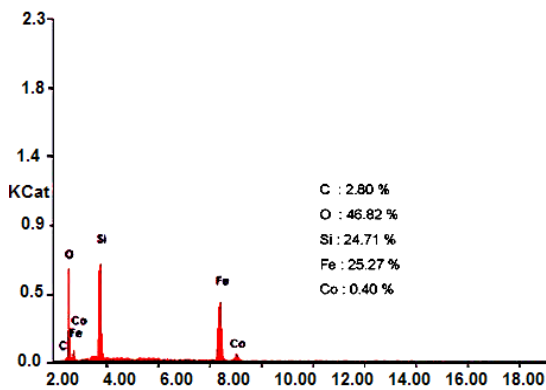


Fig. 3. Graphic percentage content of $\text{Fe}_2\text{O}_3/\text{SBA-15}$ sample

Table 2 shows that the surface area of SBA-15 and $\text{Fe}_2\text{O}_3/\text{SBA-15}$ by BET amounted to $556 \text{ m}^2 \text{ g}^{-1}$ and $470 \text{ m}^2 \text{ g}^{-1}$. While the surface area by BJH of SBA-15 and $\text{Fe}_2\text{O}_3/\text{SBA-15}$ amounted to $515 \text{ m}^2 \text{ g}^{-1}$ and $401 \text{ m}^2 \text{ g}^{-1}$. This is also reflected in the pore volume of SBA-15 and $\text{Fe}_2\text{O}_3/\text{SBA-15}$ is 1.02 cc g^{-1} and 0.87 cc g^{-1} . It shows that pore diameter decrease amounts from 8.76 nm to 6.50 nm .

These results indicate that the modification process has been successfully carried out. Montiel-Palacios (2009) stated that the doping iron particle on the surface of mesoporous silica causes the surface area of mesoporous silica decreased²³. The decrease was due to the treatment of impregnation and thermal processes that accompany it.

Table 1: Peak Assignment of FTIR Spectra of Fe_2O_3

Fe_2O_3 Peak assignment	$\text{Fe}_2\text{O}_3/\text{SBA-15}$											
	Peak	Intensity	Corr. Intensity	Base (H)	Base (L)	Area	Peak	Intensity	Corr. Intensity	Base (H)	Base (L)	Area
Fe-O	495.73	40.89	0.6	504.41	493.8	4.05	458.11	56.06	2.03	502.48	454.26	0.52
Fe-O-Si	676.08	42.07	0.15	677.04	611.46	21.96	678.01	83.18	0.18	749.38	676.08	0.05
Fe-O-Fe	863.18	63.84	0.11	868	861.25	1.31	805.32	88.75	0.15	810.14	803.39	0.01
Si-O-Si asymmetric	1001.1	77.51	0.1	1042.57	1000.13	4.28	1085.01	59.39	0.64	1346.37	1081.15	0.09
C-H bend	1384.95	76.89	0.63	1390.74	1342.51	5.2	1383.98	93.57	0.32	1394.59	1376.27	0.01
C = C aliphatic	1618.35	47.61	27.65	1736.97	1499.72	44.66	1635.71	87.51	1.48	1646.32	1569.16	0.24
-OH	3416.08	23.253	0.15	3436.33	3411.26	15.79	3443.08	68.16	0.38	3667.8	3438.26	1.66

Table 2: The BET characterization results of SBA-15 and $\text{Fe}_2\text{O}_3/\text{SBA-15}$

Properties	Samples	
	SBA-15	$\text{Fe}_2\text{O}_3/\text{SBA-15}$
Surface area by BET (m^2g^{-1})	556	470
Surface area by Langmuir surface area (m^2g^{-1})	102.6	687
Surface area by BJH method cumulative desorption surface area (m^2g^{-1})	71	541
Surface area by DH method cumulative desorption surface area (m^2g^{-1})	73	550
Surface area by DR method micropore area (m^2g^{-1})	75	619
Surface area by BJH total surface area (m^2g^{-1})	515	401
Pore volume by BJH pore volume ($\text{cm}^3 \text{ g}^{-1}$)	1.02	0.87
Pore volume by BJH method cumulative desorption pore volume ($\text{cm}^3 \text{ g}^{-1}$)	1.33	0.93
Pore volume by DH method cumulative desorption pore volume ($\text{cm}^3 \text{ g}^{-1}$)	1.33	0.91
Pore volume by DR method micropore volume ($\text{cm}^3 \text{ g}^{-1}$)	0.26	0.22
Pore volume by HK method cumulative pore volume ($\text{cm}^3 \text{ g}^{-1}$)	0.44	0.29
Pore volume by SF method cumulative pore ($\text{cm}^3 \text{ g}^{-1}$)	0.45	0.29
Pore size by diameter pore BJH (nm)	8.76	6.5
Pore size by BJH method desorption pore Radius (Mode $Dv(r)$) (nm)	3.3	3.2
Pore size by DH method desorption pore Radius (Mode $Dv(r)$) (nm)	3.3	3.2
Pore size by DR method micropore Half pore width (nm)	1.8	1.4
Pore size by DA method pore Radius (Mode) (nm)	1.1	0.9
Pore size by HK method pore Radius (Mode) (nm)	0.22	0.22
Pore size by SF method Radius (Mode) (nm)	0.22	0.22

Note : BJH (Barret-Joyner-Halenda Method), DH (Dollimore Heal Method), DR (Dubinn-Radushkevich Method), DA (Dubinin Astakhov Method), HK (Harvath-Kawazoe Method), SF (Saioto-Foley Method)

Figure 4 indicates that mesoporous silica has pore diameter about 8 nm. While mesoporous silica embedded with iron oxide has pore diameter about 6.50 nm. The decreasing of pore diameter was caused by blocking pore of mesoporous silica with iron oxide. The structure of mesoporous silica materials has not destructed by iron oxide particles. Embedding iron oxide caused the surface area of mesoporous silica decrease amounts 86 m²/g (Tabel 2). It shows that the surface area of mesoporous silica has been covered by iron oxide about 15%. There were differences between the results with the experimental plan. However, it did not make a significant difference. So, the iron oxide covering process in mesoporous silica has been successfully applied to the experiment. The results were supported by the data on the EDX, FTIR, XRD and TEM.

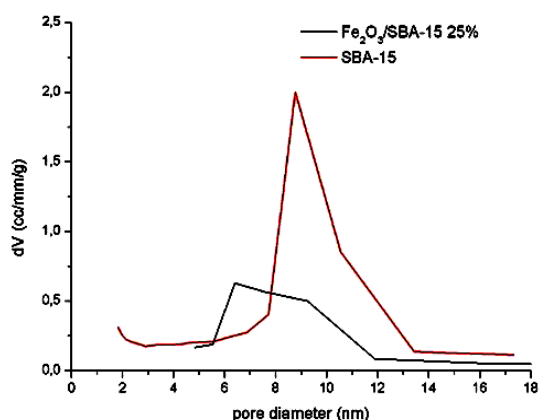


Fig. 4. Particle size distribution graph on mesoporous silica and mesoporous silica embedded with iron oxide

Based on the Fig. 5a, TEM characterization test results show that iron particle successfully distributed on mesoporous silica surface. The illustration of the iron distribution onto mesoporous silica pipe (Fig. 5b) indicates that iron particle covered the small part of mesoporous silica surface. This phenomenon have great agreement with the EDX result (Fig. 3). The covering iron phenomena could be indicated by the number of black dots on the images indicating the presence of iron particle in the surface of SBA-15. These results are supported by the data FTIR, XRD, EDX and BET also showed that iron particle has been successfully doped on SBA-15. Modification of mesoporous silica with iron oxide particles does not change the hexagonal structure of mesoporous silica (SBA-15)²³.

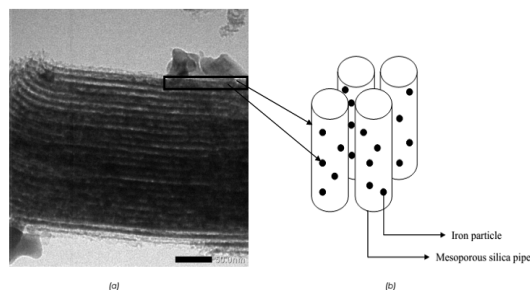


Fig. 5. Microimage of TEM in material of Fe₂O₃/SBA-15 : (a) TEM characterization result and (b) mesoporous silica pipe

Based on the results of material characterization mesoporous silica and mesoporous silica embedded with iron oxide shows the data related to each other. In the XRD results are the peaks of mesoporous silica, iron oxide, and mesoporous silica embedded with iron oxide. The peaks are used to determine the structure of the material Fe₂O₃/SBA-15 is in the form of hexagonal. This is supported by the data EDX and FTIR. The data of EDX contained on the group Si, Fe, and O which indicates that iron oxide doping process has been successfully performed on mesoporous silica. The results also have been suitable obtained by mesoporous silica embedded iron oxide (Fe₂O₃/SBA-15). These results are supported by data FTIR, which based on the data of FTIR showed their peak of Si- O-Si and Fe-O-Si. These results indicate the replacement of silicon (Si) by iron (Fe). The results of characterization BET and TEM showed the same results. BET results show that the pore diameter decreases which indicates that the doping process is successful. This is supported by data TEM (Fig. 5), which is based on images showing the black dots which indicate iron particle distribution on mesoporous silica surface.

Cadmium (II) ion adsorption pattern with the mesoporous silica embedded with iron oxide was tested with four adsorption kinetics model, Lagergren, Ho and McKay, Langmuir and Freundlich models.

Table 3: Kinetics Model Adsorption of Cadmium (II) Ion On Fe₂O₃/SBA-15

Kinetics Model	Formula	Linearity
Lagergren	$q_e = \frac{e^{kt}}{q_e - q_t}$	0.93
Ho and McKay	$q_e = \frac{(q_e - q_t)}{1 - (q_e - q_t)kt}$	0.04
Langmuir	$q_e = \frac{q_t \cdot b C_e}{1 + b C_e}$	0.91
Freundlich	$q_e = K_f \cdot C_e^{1/2}$	0.92

Figure 6 shows the kinetics trend during cadmium adsorption using Fe₂O₃/SBA-15 sample according to Lagergren model, Ho and McKay model, Langmuir model, and Freundlich model. Based on the data of test results in Table 3, the adsorption kinetics has been great fitted by Lagergren model. The Lagergren model adsorbed cadmium (II) ion onto Fe₂O₃/SBA-15 have linearity and adsorption capacity up to 0.93 and 74.25 mmol/g respectively. The high adsorption capacity appeared by mesoporous site which accessible for cadmium (II) ion.

The variations of contact time also caused the affect for the experiment. The effect of the contact time is determined by the variation of 10, 30, 60, 120, 180 and 420 with a volume of 25 mL, a mass of 0.005 g Fe₂O₃/SBA-15 at room temperature (25°C).

Fig. 6 shows the adsorption data is stable at 60 min, 120 min, and 180 min with the adsorption capacity 74.00 mmol/g; 74.25 mmol/g; and 74.78 mmol/g or approximately 61.73%; 61.95%; and 62.39% respectively. The contact time optimum at 80 min. Due to the good interaction between mesoporous silica embedded with iron oxide as adsorbent and cadmium (II) ion as adsorbate. The equilibrium point reached at 120 min and being constant after it because cadmium (II) ion has been trapped by mesoporous sites. As a sum, the optimum contact time for cadmium (II) ion adsorb onto mesoporous silica embedded with iron oxide obtained at 80 min, so mesoporous silica embedded with iron oxide could be the best material for heavy metal removal in the future.

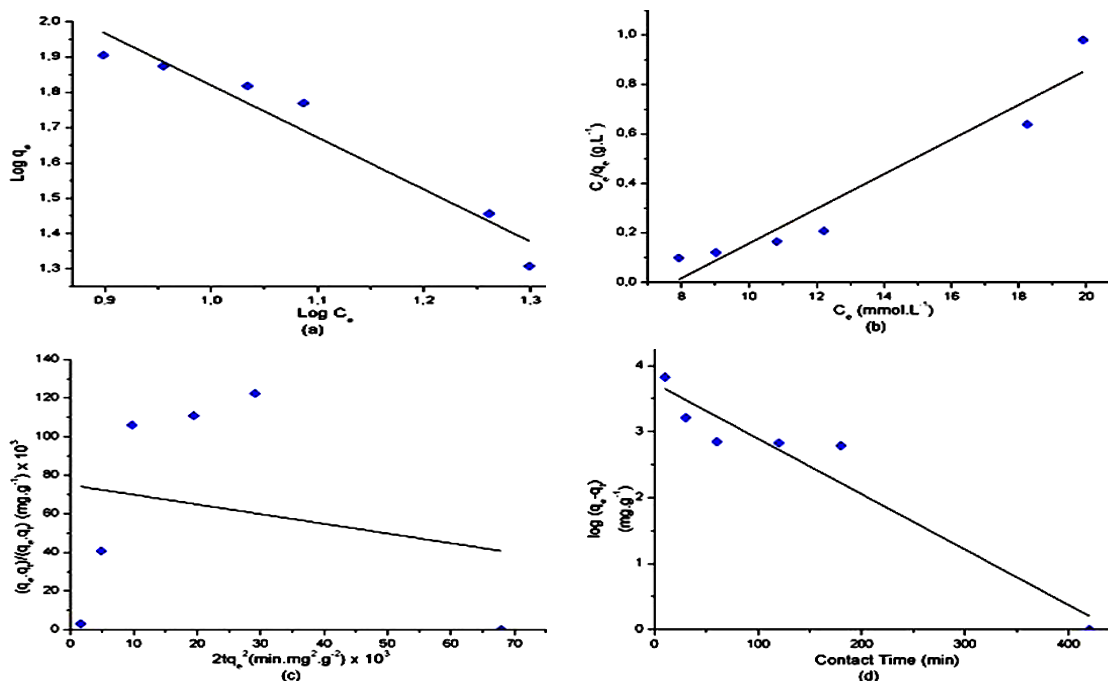


Fig. 6. Kinetics Trend during Cadmium (II) ion Adsorption using Fe₂O₃/SBA-15 : (a) Freundlich model, (b) Langmuir model, (c) Ho and McKay model, (d) Lagergren model

CONCLUSION

Mesoporous silica has been successfully embedded with iron oxide that has high magnetic properties with the wet impregnation method and microwave as adsorbent for the adsorption of cadmium (II) ion. Mesoporous silica embedded with iron oxide was characterized by X-ray diffraction and

TEM. It has the geometrical hexagonal structure with surface area, pore volume and pore diameter of 470 m² g⁻¹, 0.87 cc g⁻¹ and 6.50 nm, respectively. The content of mesoporous silica embedded with iron oxide can be seen in the results of EDX characterization with the iron particle content in the mesoporous silica embedded with iron oxide amounted to 25.47 wt%. The functional group

associated with the adsorbent showed peaks of Si-O-Si at 1085 cm^{-1} and group Fe-O-Si at 678 cm^{-1} . The kinetic model of mesoporous silica embedded with iron oxide adsorbed cadmium (II) ion follows the first order kinetics model by Lagergren. The optimum adsorption capacity of cadmium reached after a contact time of 80 min, the concentration of the adsorbate was 74.25 mmol g^{-1} with the

initial concentration of 23.97 mmol L^{-1} .

ACKNOWLEDGEMENT

Financial support from the Sebelas Maret University from PNPB Program 2019 in Scheme Research Group Capacity Building Research (Penelitian Peningkatan Kapasitas Riset Group (PPKGR) , is gratefully acknowledged.

REFERENCES

- Feng, Y.; Gong, J.L.; Zeng, G.M.; Niu, Q.Y.; Zhang, H.Y.; Deng, J.H.; Yan, M. *J. Chem. Eng.*, **2010**, *162*, 487.
- Ammari, T. G.; Al-Labadi, I.; Tahboub, A.; Ghrair, A. *Protein Environ. Saf. Process.*, **2013**, *95*, 77–85.
- Cai, C.; Zhang, Z.; Zhang, H. *J. Hazard. Mater.*, **2016**, *313*, 209–218.
- Parmar, M.; Thakur, L. S. *Int. J. Plant Sci.*, **2013**, *3*, 143–157.
- Zeinali, A.; Tow, J.; Sahebdehfar, S. *Microporous Mesoporous Mater.*, **2016**, *236*, 1–12.
- Shibiao, W.; Kaisheng, Z.; Xuelong, W.; Yong, J.; Bai, S.; Tao, L.; Fanli, M.; Zhen, J.; Dongyue, L.; Wei, S.; Lingtao, K.; Jinhuai, L. *J. Chem. Eng.*, **2015**, *262*, 1292–1302.
- Alvand, M.; Shemirani, F. *Microchim Acta.*, **2014**, *181*, 181–188.
- Atar, N.; Olgun, A.; Wang, S. *J. Chem. Eng.*, **2012**, *192*, 1–7.
- Chatterjee, A.; Schiewer, S. *J. Chem. Eng.*, **2014**, *244*, 105–116.
- Duan, J.; Su, B. *J. Chem. Eng.*, **2014**, *246*, 160–167.
- Chávez-Guerrero, L.; Rangel-Mendez, R.; Munoz-Sandoval, E.; Cullen, D.A.; Smith, D.J.; Terrones, H.; Terrones, M. *Water Res.*, **2018**, *42*, 3473–3479.
- Izidoro, J. D. C.; Fungaro, D. A.; Abbott, J. E.; Wang, S. *Fuel*, **2013**, *103*, 827–834.
- Manasi; Rajesh, V.; Kumar, S. K. A.; Rajesh, N. *J. Chem. Eng.*, **2014**, *235*, 176–185.
- A. Saeed and M. Iqbal. *Water Res.*, **2003**, *37*, 3472–3480.
- Sriyanti, C. Azmiyawati, and Taslimah. *J. Sci. Appl. Chem.*, **2005**, *8*, 1–12.
- Z. Wu and D. Zhao. *Chem. Commun.*, **2011**, *47*, 3332–3338.
- Ridhawati, A. W. Wahab, N. La Nafie, and I. Raya, *J. INTEK.*, **2018**, *5*, 39–43.
- H. Chaudhuri, S. Dash, and A. Sarkar, *J. Environ. Chem. Eng.*, **2015**, *3*, 2866–2874.
- J. L. Bonardet, S. Casale, A. Davidson, G. Andr, F. Porcher, and I. Gr. *J. Phys. Chem.*, **2012**, *116*, 3437–3448.
- P. Shukla, S. Wang, H. Sun, H. Ang, and M. Tadé, *J. Chem. Eng.*, **2010**, *164*, 255–260.
- A. R. Martins, I. T. Cunha, A. A. S. Oliveira, and F. C. C. Moura. *J. Chem. Eng.*, **2017**, *318*, 189–196.
- Sungkono, H.; Darminto. *J. Phys. and App.m.*, **2006**, *2*, 1–5.
- Z. Luan, Hartmann, M.; Zhao, D.; Zhao, W.; and L. Kevan. *Chem. Mater.*, **1999**, *11*, 1621–1627, 1999.
- M. Ulfa, R. M. Hasanah, and D. Prasetyoko, *IOP Journal of Physic.*, **2018**, *020001*, 1-7.
- M. Ulfa, W. Trisunaryanti, I. Falah, and I. Kartini, *Chem. Eng. Rev.*, **2016**, *9*(09), 588–597.
- M. Ulfa, K. S. Aristia, D. Prasetyoko, M. Ulfa, K. S. Aristia, and D. Prasetyoko, *Journal of Physic IOP*, **2018**, *020002*, 5-14.
- M. Ulfa, W. Trisunaryanti, I. I. Falah, and I. Kartini, “Characterization of Gelatines Extracted From Cow Bone for Carbon Synthesis.”, **2015**, *8*(8), 57–63.
- M. Ulfa, W. Trisunaryanti, I. I. Falah, and I. Kartini, *Indones. J. Chem.*, **2016**, *16*(3)239–242.
- R. Ediati, M. Ulfa, H. Fansuri, Z. Ramli, and H. Nur, *J. Fund. Mat. Tech.*, **2014**, *46*(1), 76–90.
- M. Ulfa and D. Prasetyoko, *Orient. J. Chem.*, **2018**, 1–6.
- M. Ulfa and A. M. Jannah, *Orient. J. Chem.*, **2018**, *34*(1), 420–429.